

Contents lists available at ScienceDirect

Combustion and Flame

journal homepage: www.elsevier.com/locate/combustflame



Plasma-based global pathway analysis to understand the chemical kinetics of plasma-assisted combustion and fuel reforming



Praise N. Johnson, Taaresh S. Taneja, Suo Yang*

Department of Mechanical Engineering, University of Minnesota - Twin Cities, Minneapolis, MN 55455, USA

ARTICLE INFO

Article history: Received 22 October 2022 Revised 26 June 2023 Accepted 26 June 2023 Available online 5 July 2023

Keywords: Global pathway analysis (GPA) Plasma assisted combustion (PAC) Fuel reforming Ammonia combustion Methane reforming Global reaction pathways

ABSTRACT

The Global Pathway Analysis (GPA) algorithm helps analyze the chemical kinetics of complex combustion systems by identifying important global reaction pathways connecting a source species to a sink species through various important intermediate species (i.e., hub species). The present work aims to extend GPA algorithm to plasma-assisted combustion and fuel reforming systems to identify the dominant global pathways in such systems at various conditions. In addition, the present study extends the ability of GPA algorithm to identify reaction cycles involving the excitation of high-concentration species (e.g., O2, N2, and fuel) to their vibrational and electronic states and the subsequent de-excitation to their ground state, based on their significance on the reactivity of plasma-assisted systems in terms of gas heating and radical production. Provisions are made in the GPA algorithm to evaluate the reactivity of identified reaction pathways and cycles based on the element-flux transfer (i.e., dominance), heat release, and radical production rate. The newly developed Plasma-based Global Pathway Analysis (PGPA) algorithm is then used to analyze the plasma-assisted combustion of ammonia and reforming of methane. The PGPA analyses elucidated the significance of vibrational-translational cycles on the reactivity of NH3/air mixtures. Further, analyses on the production of NO ascribed the early reforming of NH3 to N2 and H2 in impeding the production of NO during plasma-assisted NH₃ ignition. Lastly, the enhanced reforming of CH₄/N₂ mixtures using plasma has been attributed to electron impact dissociation of CH₄ when compared to thermal reforming. In contrast, conventional path-Flux analysis (PFA) was found to require significant manual effort and pre-analysis intuitions from expert knowledge, making it arduous to provide valuable insights into plasma chemistry. The user-friendly and automated nature of PGPA thus provides a valuable tool for assessing the kinetics of plasma-assisted systems helpful in analyzing and, further, a foundation in reducing plasma-assisted chemistry, without the needs of expert knowledge.

© 2023 The Combustion Institute. Published by Elsevier Inc. All rights reserved.

1. Introduction

Plasma-assisted combustion/reforming (PAC/PAR) systems provide an unparalleled opportunity to improve the ignition, flame stabilization, and emission characteristics of combustion systems [1–6]. Plasma discharges, resulting in the production of charged particles (electrons and ions) and various excited species, can catalyze the production of radicals in the PAC system, thereby enhancing the reactivity and heat release [7]. In PAR systems, these electrons and excited species aid in the decomposition of fuel to smaller radicals, promoting the formation of a reformed reactive gas mixture [6,8]. The plasma chemistry involves many new reaction classes such as electron impact ionization, excitation, dissociative excitation, dissociative ionization, dissociation, de-excitation,

* Corresponding author.

E-mail address: suo-yang@umn.edu (S. Yang).

attachment, and recombination reactions [7]. These new classes of reactions governing the plasma kinetics are then coupled with conventional combustion kinetics to construct the detailed PAC/PAR chemistry [7,8]. The inclusion of plasma reactions, whose rates depend on the reduced electric field (E/N) and cross sections of the colliding species, introduce additional complexity to the previously intricate combustion kinetics. These complexities, along with the considerably large size of the coupled PAC/PAR mechanisms, presents a formidable endeavor in obtaining beneficial insights into the kinetics of plasma-assisted systems even using a zero-dimensional (0D) model.

Several methods exist in the literature [9–18] to identify the aggregate behavior during the course of fuel oxidation using detailed combustion chemistry. The foremost among these methods is Computational Singular Perturbation (CSP) [9], which analyzes the chemical behavior of the system by decoupling timescales and reaction kinetics, thereby grouping the reactions into differ-

ent classes based on timescales. The decoupling of fast time scales can also be performed using Intrinsic Low Dimensional Manifolds (ILDM) [13], based on an eigen-analysis of the governing chemical equations. In addition, Lu et al. [16] developed a Chemical Explosive Mode Analysis (CEMA) tool to identify the different explosive modes assisting the understanding of ignition and flame structure. Won et al. [17] introduced the concept of a transportweighted enthalpy and a radical index to quantify the effect of mass transport and chemical kinetics on diffusion flame extinction. More recently, Zhong et al. [19] investigated the eigenmodes of thermal-chemical instability involving different plasma energy transfer processes and chemical reactions in a OD plasma system. However, the aforementioned timescale-based methods do not identify the process of fuel oxidation to final products and the important reaction pathways governing the same. The importance of different reactions on specific combustion parameters (e.g., ignition delays, flame speeds, etc.) can be gauged using sensitivity analysis [18] by perturbing the reaction rate constant of each reaction and probing its effect on the parameter. Nevertheless, sensitivity analysis is a brute-force method as it involves a simulation for each perturbed reaction, thereby demanding a significant computational effort to analyze the detailed chemistry. Thus, it is necessary to delve into lesser computationally-demanding methods that realize the important reaction pathways governing the fuel

Gao et al. [20,21] developed a graph-based Global Pathway Analysis (GPA) algorithm to identify the global reaction pathways connecting a source and sink species based on atomic flux quantification. The algorithm involves the construction of an element flux graph, followed by the identification of certain important species (i.e., hub species) based on a critical atomic flux crossing, and subsequently identifying the global pathways for each identified hub species. GPA algorithm presents a way to relate all the conversion steps from the initial fuel (i.e., source) to the final product (i.e., sink), whereas, the conventional Path-Flux Analysis (PFA) method [22] just considers one or two conversion steps at a time. Therefore unlike PFA and timescale-based methods, the global pathways identified using GPA describes the overall conversion chemistry of fuel to products and thus, can be used to analyze and describe the importance of specific reactions or species in governing the chemistry. Studies [20,21,23-25] also utilized GPA to analyze the combustion chemistry of auto-ignition in 0D batch reactors and the local extinction and re-ignition of 3D turbulent nonpremixed flames and further, in reducing the combustion mechanisms using identified global pathways. In addition to these conventional GPA studies, Mishra et al. [26] proposed an adaptive global pathway selection algorithm using artificial neural networks to improve the accuracy of predictions of reduced mechanisms at reduced computational costs.

Recently, Zhou et al. [27] extended the application of GPA to soot chemistry, by considering the element fluxes of carbon atom from polycyclic aromatic hydrocarbons (PAHs) to soot, allowing to probe the different soot production pathways in detailed soot kinetics. Similarly, Johnson et al. [28] probed into the possibility of accommodating PAC chemistry in the existing GPA algorithm by considering both plasma and conventional combustion reactions. Nevertheless, Johnson et al. [28] observed the necessity in improving the GPA algorithm to account for the various special effects in the PAC chemistry. For example, the gas heating due to excitation and de-excitation of certain species (e.g., $N_2 \longrightarrow N_2^* \longrightarrow N_2$, with N₂* being a general representation of any electronic or vibrational excited state of N2) are found to greatly influence the plasmaassisted ignition [28,29]. The conventional GPA, when simply implemented to identify global pathways in plasma assisted systems, does not capture the excitation-deexcitation cycles and their associated effects on the reactivity of the systems.

The present study aims to develop a Plasma-based Global Pathway Analysis (PGPA) algorithm for plasma-assisted combustion and fuel reforming systems by accounting the aforementioned effects. The highlights of the present study are three-fold: (1) An algorithm to identify the global pathways and excitation-deexcitation cycles involved in the kinetics of plasma-assisted systems; (2) Insights into the various effects of each pathway/cycle such as gas heating, radical production, and dominant fuel-consuming channels; (3) Application of the newly developed PGPA to the PAC of ammonia (NH₃) and PAR of methane (CH₄), identifying the global reaction channels governing the reactivity and fuel reforming. This work is among the first to comprehensively propose a methodology to investigate the chemical kinetics of plasma-assisted systems, by considering both cyclic reactions and global conversion routes in an accessible and automatic manner. Bellemans et al. [30,31], in their studies, extended the application of Directed Relation Graph with Error Propagation (DRGEP) and Principal Component Analysis (PCA) to obtain reduced kinetic mechanisms for plasma-assisted chemistry. Regardless, Gao et al. [20,21] observed the GPA-based reduction to provide better error control over DRGEP-based reduction for similar sized reduced mechanisms. Thus, in addition to providing an analysis methodology for plasma systems, the PGPA formulation can be further used to develop mechanism reduction strategies with finer error control for plasma assisted systems, complementing the existing efforts in the literature [30,31].

The current article is organized as follows. Section 2 presents the methodology involved in the development of PGPA algorithm. Section 3 describes the methods used for numerical simulation of plasma-assisted systems. The simulation results of PAC of NH₃ and PAR of CH₄, along with the analyses using the newly developed PGPA, followed by the discussion and comparison against conventional path-flux analysis are presented in Section 4. Following the analyses and discussions, the conclusions are summarized in Section 5.

2. Plasma-based global pathway analysis (PGPA)

A detailed description of GPA to identify global pathways for conventional combustion systems can be found elsewhere in the literature [20,21,27]. Nevertheless, the approach to identify global pathways of plasma-assisted systems is discussed here (Section 2.1) for completeness of the study. Subsequently, the method to identify the excitation-deexcitation cycles will be presented in detail (Section 2.2) along with the different effects of the global pathways and cycles (Section 2.3).

2.1. Identification of global reaction pathways

Global reaction pathways for a plasma-assisted system are identified based on the approach suggested by Gao et al. [20,21]. Firstly, an element flux graph is constructed for an element of interest (C, H, N, etc.) with each node of the graph representing a species and the edges connecting the nodes depicting the element flux between the two nodes. The element flux of the *e*th element going from the *i*th species to the *j*th species ($A_{e,i odder j}$) is given by

$$A_{e,i\to j} = \sum_{r} a_{e,r,i\to j},\tag{1}$$

where, $a_{e,r,i\rightarrow j}$ represents the element flux of the eth element going from the ith species to the jth species by means of the rth reaction. In Eq. (1), $a_{e,r,i\rightarrow j}$ is obtained by

$$a_{e,r,i\to j} = \max(0, C_{e,r,i\to j}\dot{\omega}_r). \tag{2}$$

In Eq. (2), $\dot{\omega}_r$ represents the reaction rate of the *r*th reaction, while $C_{e,r,i\rightarrow j}$ gives the elemental flux from the *i*th species to the *j*th species proceeding through the *r*th reaction and is given by Eq. (3).

The positive elemental flux from the *i*th species to the *j*th species alone are considered to calculate $a_{e,r,i\rightarrow j}$.

$$C_{e,r,i \to j} = \begin{cases} n_{e,r,j} \frac{n_{e,r,i}}{n_{e,r}}, & \text{if } \nu_{r,j} \nu_{r,i} < 1; \\ 0, & \text{otherwise.} \end{cases}$$
 (3)

In Eq. (3), $n_{e,r,i}$ represents the number of the eth element going out from the ith species in the rth reaction, and $n_{e,r,j}$ represents the number of the eth element going into the jth species in the rth reaction. A negative value of $v_{r,j}v_{r,i}$ (with v being the stoichiometric coefficient) ensures the presence of ith and jth species at the opposite ends of a reaction, thereby enabling the transfer of the eth element from the ith species to the jth species through the rth reaction. When $v_{r,j}v_{r,i}>0$, both the ith and jth species are present on the same side of the rth reaction and therefore, a zero element transfer is ensured between the two species.

The element flux graph generated using the aforementioned methodology contains both combustion and plasma species as nodes. The element flux involving plasma species can be calculated using the rate expressions for plasma reactions generated by a standard Boltzmann equation solver like BOLSIG+ [32]. At this juncture, several important species named 'hub species' are identified in the event of a normalized element flux going out or coming into the species is greater than a user-specified threshold (α_{crit}):

$$\frac{\max\left(\sum_{k}a_{e,i\rightarrow k},\sum_{k}a_{e,k\rightarrow i}\right)}{\max_{M}\left[\max\left(\sum_{k}a_{e,M\rightarrow k},\sum_{k}a_{e,k\rightarrow M}\right)\right]}\equiv\alpha_{e,i}\geq\alpha_{crit}.$$
(4)

As the value of α_{crit} is increased to a higher element-flux threshold, the number of identified hub species decreases. For each hub species, the global reaction pathways connecting a source species (often fuel species) to a sink species (any intermediate or product species) through the hub species are obtained by identifying the fastest chemical reaction pathways to transfer atoms from the source to sink species through the hub species. The procedure of obtaining the shortest pathways for all hub species has been explained in Gao et al. [20,21]. The global pathways are ensured to be devoid of any cycles and repetitive steps so as to obtain simple pathways with no repeated vertices.

2.2. Identification of cyclic reaction channels

The coupled plasma-assisted combustion/reforming kinetics consist of electrons, charged species (e.g., N2+), and radicals (e.g., OH). In addition, PAC kinetics also contain neutral species such as conventional combustion species (ground state species like N2) and species at excited states (e.g., N2, a general representation of any excited state of N₂). Since the global reaction pathways identified by GPA are simple pathways with no repeated nodes, the cyclic reaction steps involving the ground and excited states (e.g., $N_2 \longrightarrow N_2^* \longrightarrow N_2$) will never appear in global pathways. However, the excitation of a ground state species followed by its de-excitation back to the ground state can be of greater importance as these cyclic reaction steps can result in significant gas heating and radical production thereby improving the reactivity of the system [28,29,33–35]. Thus, it is imperative to identify the important excitation-deexcitation cycles (simply referred to as 'cycles' hereafter) and their effects on the reactivity of plasma-assisted systems.

The current study employs a modified version of Depth First Search (DFS) algorithm to find all the cycles (pathways with source and sink being the same) involving a ground state species (S_0) and their corresponding excited species (S_i) , with i representing the ith excited state) by utilizing the element-flux graph. A schematic of the modified DFS algorithm implemented in the present work is shown in Fig. 1. Starting with S_0 , the algorithm checks for excited states of S_0 in each adjacent node. In the instance of identifying

an excited state species (say S_i), S_i is added to the cycle string (a sequence of steps identified in the current search) and the procedure is repeated recursively to check the adjacent nodes of S_i . The recursive search is repeated until one of the adjacent node is matched to the ground state S_0 . If the search for adjacent node terminates without reaching the ground state or another excited state, the algorithm reverts to the previous excited state and the search is continued for a different adjacent node. Provisions are made in the DFS algorithm to detect the occurrence of repeated nodes and discard if any, in order to avoid infinite recursions. The cycle identified will be of the form $S_0 \longrightarrow S_1 \longrightarrow \ldots \longrightarrow S_i \longrightarrow S_j \longrightarrow \ldots \longrightarrow S_0$, where $S_i \longrightarrow S_j$ represents all possible conversion steps between the excited states of S_0 .

Figure 2 depicts a representation of an element flux graph and the concept of cycles identified in the present work. The species P denotes any species which is not an excited state of S_0 . It is shown that the reaction sequence $S_0 \to P \to \ldots$ and $S_0 \to S_i \to S_j \to P \to \ldots$ are not identified as cycles owing to the presence of species P in those sequence. In addition, the sequence $S_0 \to S_i \to S_j \to S_k \to S_i \to S_j \to S_k \to \ldots$ is also discarded as, this sequence forms an infinite cycle with a recurring repetition of species in a specific order (repetition of $\to S_i \to S_j \to S_k \to S_k \to S_i \to S_j \to S_k \to S_k \to S_j \to S_k \to S_k$

2.3. Effects of global reaction pathways and cycles

The use of PGPA to obtain global reaction pathways and cycles explained in Sections 2.1 and 2.2 can result in the identification of countless possible combinations of pathways and cycles. To understand the relative importance of the identified pathways and cycles, it is necessary to rank them based on quantifiable parameters that relates to reactivity.

2.3.1. Element flux dominance

To understand the behavior of the plasma-assisted system, it is necessary to find the dominant pathways governing the consumption of the source species. Gao et al. [21,23] defined the factor 'dominance' ($D_{GP,e}$) for each global pathway (GP) based on the element flux transfer through that pathway. $D_{GP,e}$ represents the fraction (a value between 0 and 1) of the eth element that gets transferred through the global pathway of interest and is given by

$$D_{GP,e} = D_{source,e} D_{GP/source,e}, \tag{5}$$

where $D_{source,e}$ is the ratio of total number of the eth atom in the source species to the total number of the initial eth atom and is given by Eq. (6):

$$D_{source,e} = \frac{n_{source,initial} N_{source,e}}{\sum_{i} n_{i,initial} N_{i,e}}.$$
 (6)

In Eq. (6), $n_{i,initial}$ represents the initial number of moles of the ith species and $N_{i,e}$ represents the number of the eth atom present in one mole of the ith species. $D_{GP/source,e}$ represents the fraction of the eth atoms going from the source to the sink through the global pathway of interest. This is expressed in Eq. (7) as a geometric mean of the fractions of the eth atoms distributed to the conversion steps of this global pathway, in which n_{GP} represents the number of conversion steps in the global pathway.

$$D_{GP/source,e} = \left(\prod_{i,i \in GP} \frac{A_{e,i \to j}}{\sum_{k} a_{e,i \to k}}\right)^{\frac{1}{n_{GP}}}$$

$$\tag{7}$$

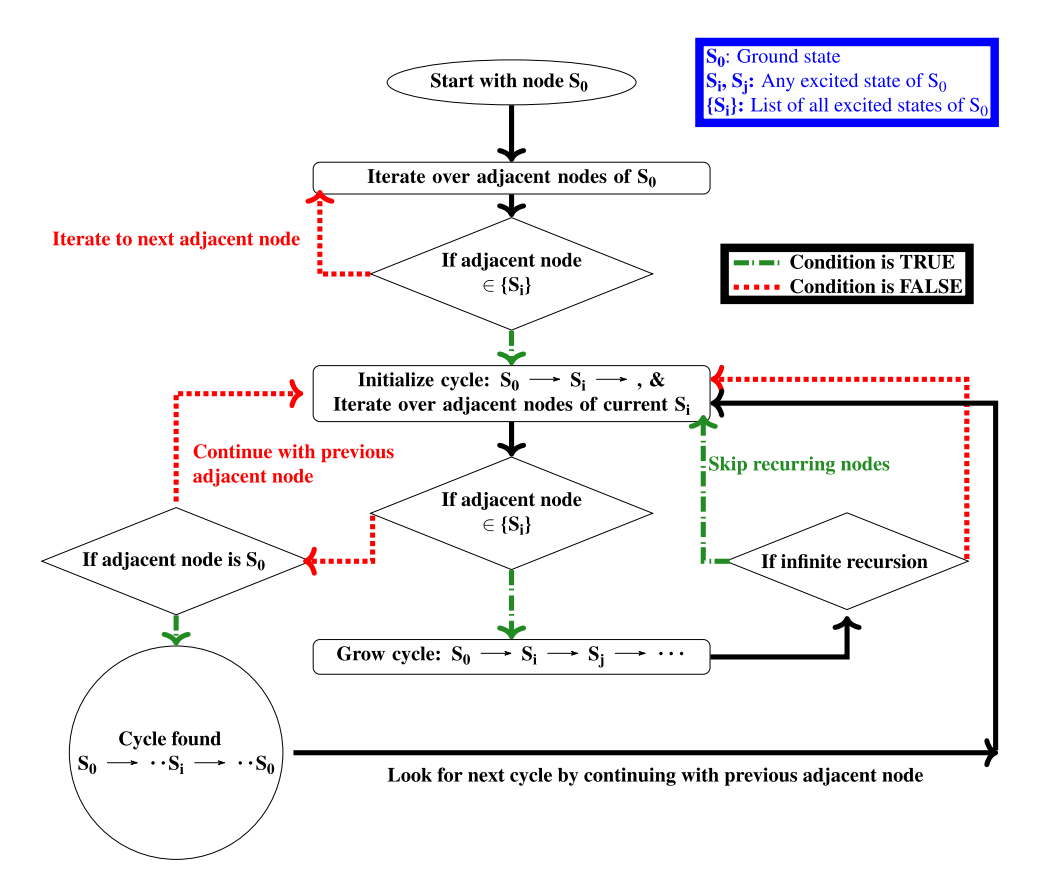


Fig. 1. Implementation of a modified Depth First Search (DFS) algorithm to find all the cycles in the current study.

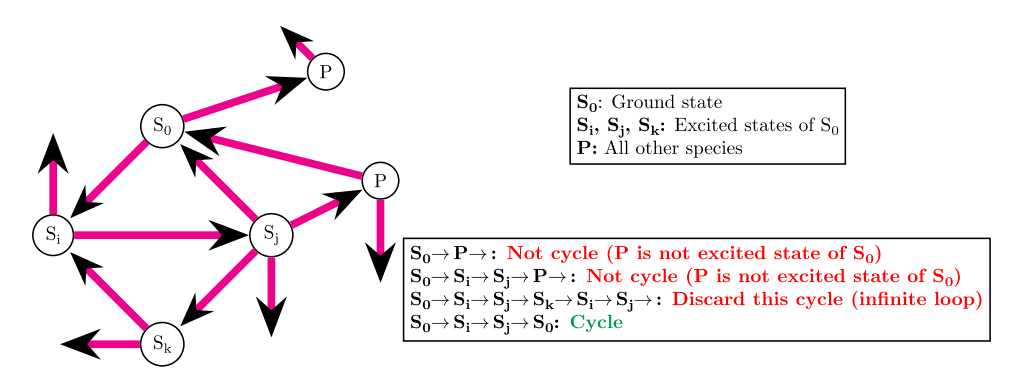


Fig. 2. A representation of an element flux graph involving ground state (S_0) , excited states $(S_i, S_j, \text{ and } S_k)$, and other species (P). The reaction sequences shown in box indicates the definition of a 'cycle' in the present study.

The GP's with the largest values of $D_{GP,e}$ are the dominant global pathways. These GP's transfer the highest flux from source to sink indicating fast consumption of the source species. In the current study, the proposition of dominance is also applied to a cycle starting at ground state S_0 (D_{Cyc,S_0}) to understand the relative importance of different cycles in terms of element flux transfer.

2.3.2. Gas heating

Combustion and plasma chemistry encompass both exothermic (i.e., heating: $\Delta h_r < 0$) and endothermic (i.e., cooling: $\Delta h_r > 0$) reactions. The heating induced by the pathway/cycle determines the gas temperature thereby affecting the reactivity of the gas mixture. Therefore, it is essential to rank the GP's and cycles based on their heat release. The electron-impact reactions impart a zero heat release/absorption, because the difference in energy levels between reactants and products is purely contributed by the change in the kinetic energy of the electrons rather than molecules, thereby lead-

ing to a change in potential energy of the molecules without releasing/absorbing heat.

A GP with source S_0 , sink $S_{n_{GP}}$, and n_{GP} steps is of the form $S_i \longrightarrow S_j$ where $i=0, 1, 2,..., n_{GP}-1$ and j=i+1. For any step $S_i \longrightarrow S_j$ in the GP, the total heat release in that step $(Q_{GP,i \rightarrow j})$ can be calculated using

$$Q_{GP,i\to j} = \sum_{r} \dot{\omega}_r \Delta h_{GP,i\to j,r},\tag{8}$$

where $\Delta h_{GP,i\rightarrow j,r}$ represents the reaction enthalpy and $\dot{\omega}_r$ is the reaction rate of the rth reaction participating in the step of $S_i \longrightarrow S_j$. $\Delta h_{GP,i\rightarrow j,r}$ is taken to be zero if the rth reaction is an electron-impact reaction. The total heating induced by the GP $(Q_{GP,e})$ is the sum of all step heating scaled by the dominance. The scaling of $Q_{GP,e}$ (or any other quantity of interest) with dominance accounts for the contribution of the respective global pathway to the total heat released. In the omission of such scaling, for a particular step

repeating in two global pathways, the same heat release will be double-counted for both pathways rather than the contribution of that step by a specific pathway. Dominance, in this case, is a measure to scale the contribution of a global path. $Q_{GP,e}$ is then given by

$$Q_{GP,e} = D_{GP,e} \sum_{i \to j} Q_{GP,i \to j}. \tag{9}$$

The above approach can also be utilized to find the heating induced by a cycle (Q_{Cyc,S_0}) by summing up the step heat releases $(Q_{Cyc,i\rightarrow j})$ and scaling with dominance of the cycle (D_{Cyc,S_0}) as shown in Eq. (10).

$$Q_{Cyc,S_0} = D_{Cyc,S_0} \sum_{i \to j} Q_{Cyc,i \to j}$$

$$\tag{10}$$

The first step of a cycle $S_0 \longrightarrow \ldots \longrightarrow S_i \longrightarrow S_j \longrightarrow \ldots \longrightarrow S_0$ is generally an electron-impact reaction $E+S_0 \longrightarrow E+S_1$, where S_1 is an excited state (vibrational or electronic). This step is considered to have zero heating, as the energy imparted by the electron is solely used to increase the potential energy of S_0 . The electron-impact relaxation of an excited species (super-elastic collision) to its ground state (e.g., $E+S_1 \longrightarrow E+S_0$) is also considered to impart zero heating, as the energy released during relaxation is only utilized to increase the mean kinetic energy of the electron. Other reactions involving the ground and excited states such as the likes of de-excitation, dissociative quenching of excited state species, and ladder-climbing reactions of the excited state species (excluding electron impact ladder-climbing) are considered to impart non-zero gas heating, proportional to their enthalpy of reaction.

2.3.3. Radical production

In addition to heat release, the global pathways and cycles affect the production of reactive radicals (e.g., O, H, and OH) during different conversion steps. An increase in the production of reactive radical pool is associated to an enhanced reactivity and faster ignition. In addition to the global pathways producing radicals, ultra-fast dissociation of $O_2 \longrightarrow 2\,O$ by the cycles involving electronically excited states of N_2 unfold additional ways to produce radical pool [34,36,37]. Thus, it is essential to understand the radical production in both global pathways and cycles to ascertain the important pathways/cycles governing the reactivity.

The production of a radical R through a GP ($P_{GP,e,R}$) or cycle ($P_{Cyc,S_0,R}$) can be calculated by summing up the radical production across all conversion steps scaled by the dominance, as shown in Eqs. (11) and (12):

$$P_{GP,e,R} = D_{GP,e} \sum_{i \to j} P_{GP,e,R,i \to j}; \tag{11}$$

$$P_{Cyc,S_0,R} = D_{Cyc,S_0} \sum_{i \to j} P_{Cyc,S_0,R,i \to j},$$
(12)

where

$$P_{GP,e,R,i\to j} = P_{Cyc,S_0,R,i\to j} = \sum_{r} \nu_{r,i\to j}^R \dot{\omega}_r, \tag{13}$$

and $\nu_{r,i \to j}^R$ represents the stoichiometric coefficient of the radical R in the rth reaction of the conversion step of interest.

In a nutshell, the PGPA algorithm identifies the global pathways and cycles along with their effects on reactivity, as shown in Fig. 3. Firstly, the element flux graph is constructed, followed by the identification of hub species based on critical flux crossing. The shortest global pathways are identified based on hub species and the cycles are identified from the graph based on a modified DFS algorithm. The quantities of dominance, gas heating, and radical production are calculated for all pathways/cycles to identify the important pathways/cycles that affect the reactivity significantly.

3. Numerical modeling of plasma-assisted systems

An in-house OD plasma-assisted combustion and fuel-reforming solver [29] is used to simulate the plasma-assisted combustion of NH₃ and reforming of CH₄ in 0D homogeneous batch reactors. The solver couples a 0D plasma kinetics code ZDPlasKin [38] with a OD combustion kinetics module based on CHEMKIN-III [39] subroutines, similar to existing studies in the literature [40,41]. The collision rate coefficients of various electron-impact reactions and the electron transport parameters are calculated by solving Boltzmann equation, which is valid for weakly ionized plasmas (the focus of present work). These calculations are done using an opensource Boltzmann equation solver named BOLSIG+ [32], by using collision cross sections as input. Nanosecond repetitive pulsed nonequilibrium plasma discharges are considered in the current study with microsecond gaps after each pulse. The duration of each pulse is varied until a targeted total value of pulse energy is deposited. The combustion chemistry is kept frozen during the pulse whereas both plasma and combustion chemistry are active during the gap. The solver employs a constant value of reduced electric filed (E/N) and hence, a square wave profile for E/N is assumed. A detailed description of the solver methodology and its validation can be found elsewhere in the literature [29,42].

A detailed kinetic mechanism for NH₃, based on our previous investigation of PAC of NH₃/air mixtures [29] is used in this study. A plasma kinetic mechanism assembled in Faingold and Lefkowitz [43] for NH₃/O₂/He mixtures was used as a reference for obtaining all the NH₃ - O₂ reactions in the mechanism used in this work. The mechanism [29] contains vibrational and electronic excited states of N₂ and O₂ along with the vibrational states of NH₃. Besides, it also considers the electron-impact dissociation of NH₃ and O₂ and ionization of NH₃, N₂, and O₂. In addition, the current study also analyzes the plasma-assisted reforming of CH₄ using PGPA, for which, the pyrolysis chemistry of CH₄/N₂/Ar/He proposed by Mao et al. [44] is chosen as the kinetic mechanism to perform the OD calculations.

4. Results and analysis

This section presents the numerical results of the plasma-assisted combustion of NH_3 (Sections 4.1 and 4.2) and plasma-assisted reforming of CH_4 (Section 4.3), along with the analyses using the newly developed PGPA. The inferences obtained from the analyses using PGPA will be compared against that obtained from conventional path-flux analysis (PFA). The dominance, gas heating, and radical production of the different global pathways and cycles obtained using PGPA will be used to ascertain their effects on the reactivity of the systems.

4.1. Effect of E/N on NH3/air ignition

Our recent study [29] numerically investigated the PAC of NH_3 /air mixtures at an initial temperature of 800 K, pressures of 1 and 3 bar, and different equivalence ratio (ϕ) mixtures under nanosecond pulsed discharges. The study analyzed the dependence of ignition and NO_x production on various parameters such as reduced electric field (E/N), ϕ , pressure, and subsequently compared the ignition using plasma discharge against a more conventional thermal energy discharge. The study observed a faster ignition at a lower E/N of 150 Td (1 Td = 10^{-17} V cm²) compared to a higher 550 Td as shown by the temperature evolution in Fig. 4(a). Using conventional path-flux analysis, at 150 Td, the vibrational-translational (V-T) relaxation vibrational-vibrational (V-V) exchange reactions of vibrationally excited states of N_2 and NH_3 were found to affect slow gas heating thereby increasing the temperature. No significant difference were observed in the radical

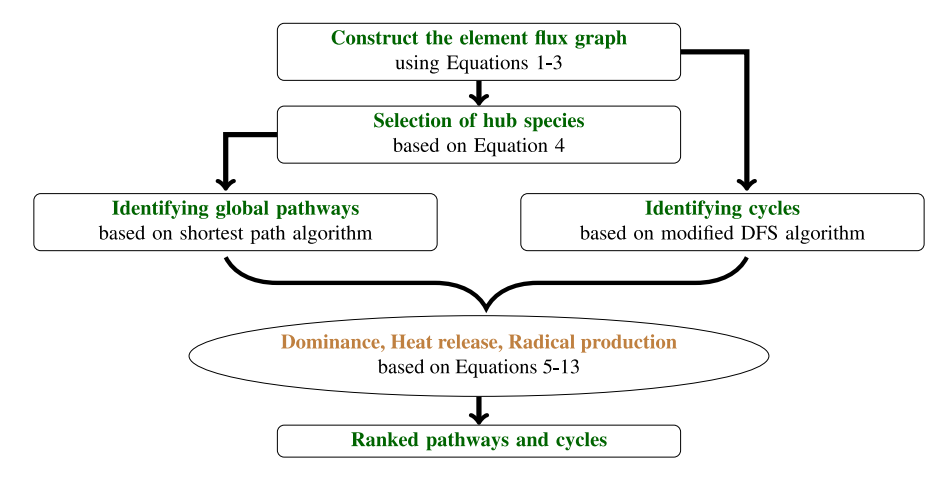


Fig. 3. The flow chart of the proposed plasma-based global pathway analysis (PGPA) algorithm.

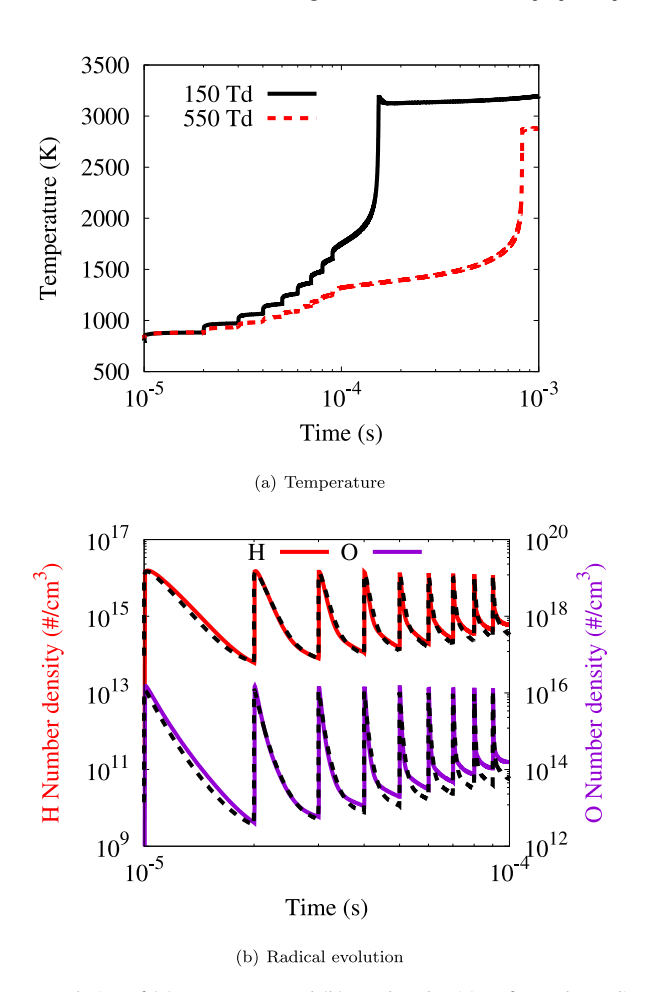


Fig. 4. Evolution of (a) temperature and (b) number densities of H and O radicals for E/N = 150 Td and 550 Td in a constant volume 0D batch reactor. In (b), the colored solid lines represents the data at 150 Td and the black dashed lines represents data at 550 Td.

evolution to possibly explain the higher reactivity at 150 Td (see Fig. 4(b)). Thus, the study attributed the higher reactivity at 150 Td to the gas heating effected by V-T and V-V reactions, and these reactions were found to be insignificant at 550 Td thereby explaining the lower reactivity at 550 Td.

To quantitatively ascertain the contribution of V-T and V-V reactions on the higher reactivity at 150 Td, the current study employs the newly developed PGPA to analyze the global pathways and cy-

cles at both 150 and 550 Td. The global pathways were identified by constructing element flux graph for N-atom, considering the source as NH₃ and sink as N₂. Besides, the PGPA was executed ensuring the analyses of all possible cycles involving O2, N2, and NH3 and their excited states. Tables 1 and 2 show the global pathways and cycles identified using PGPA along with the pathway dominance and cycle heating at 150 and 550 Td, respectively. At 150 Td, the major cycles identified were that involving the vibrationally excited states of N_2 ($N_2(v_{1-6})$) and NH_3 ($NH_3(v_2)$), as shown in Table 1. These cycles begin with an electron-impact reaction $(E + N_2 \longrightarrow E + N_2(v_{1-6}))$ followed by an exothermic de-excitation $(N_2(v_{1-6}) + M \longrightarrow N_2 + M$, where M is predominantly NH₃). On the contrary, the exothermic cycles involving electronically excited states of N2 (N2(B) and N2(C)) were found to be the most significant besides the sole V-T cycle $NH_3 \longrightarrow NH_3(v_2) \longrightarrow NH_3$ at 550 Td. These observations from PGPA indicate the dominance of vibrational species and their relaxation at 150 Td and conversely, the importance of electronically excited species and their relaxation at 550 Td. The V-T relaxation cycles foster slow gas heating over the microsecond gaps ($\sim 1416 \text{ W/cm}^3$), thereby facilitating a steady rise in temperature during the pulses and gaps at 150 Td (see Fig. 4(a)). In contrast, at 550 Td (see Table 2), the relaxation of electronic states cause fast gas heating (~ 1164 W/cm³) over nanosecond time scales during the pulses and the scant presence of V-T relaxations limit the rise in temperature during the gaps. The fast gas heating during pulse happens in a very short period when the combustion chemistry is frozen. But slow gas heating due to V-T cycles is spread over the microsecond gap where combustion chemistry is active. Thus, the primary proponent of reactivity among the two forms of heating boils down to the one with a higher heat release. Correspondingly, the 150 Td case leads to an overall faster temperature rise and faster ignition when compared to the 550 Td case.

Tables 1 and 2 also show the global pathways consuming NH_3 and producing N_2 . To validate the consumption pathways identified by PGPA, a conventional path-flux analysis (PFA) is also performed at 150 and 550 Td as shown in Fig. 5. At 150 Td, the dominant first step in consuming NH_3 is $NH_3 \longrightarrow NH_2$ followed by production of H_2NO , NNH, and NH (see Table 1). In addition, global pathways shows the production of $NH_3(v_2)$ from NH_3 , which gets consumed to produce NH_2 . Similar results can be observed from the path-flux diagram (see Fig. 5(a)), where, major consumption of NH_3 results in producing NH_2 , which further produce H_2NO , NNH, and NH. Figure 5(a) also shows the dominance of V-T relaxation of $NH_3(v_2)$, thereby resulting in significantly smaller fraction of $NH_3(v_2)$ consumed to form NH_2 . This comparison between the global pathways predicted by PGPA and conventional PFA reflects

Table 1Global pathways and cycles obtained using PGPA for the nanosecond discharge PAC of stoichiometric NH₃/air mixture at 150 Td. A positive value of heating denotes a net heat release through the pathway/cycle.

Global pathways/cycles	Parameter
Tracked by N atom	Dominance
$NH_3 \longrightarrow NH_2 \longrightarrow H_2NO \longrightarrow HNO \longrightarrow NO \longrightarrow NNH \longrightarrow N_2$	0.066
$NH_3 \longrightarrow NH_2 \longrightarrow H_2NO \longrightarrow HNO \longrightarrow NO \longrightarrow N_2$	0.054
$NH_3 \longrightarrow NH_2 \longrightarrow NNH \longrightarrow N_2$	0.053
$NH_3 \longrightarrow NH_2 \longrightarrow NH \longrightarrow N_2H_2 \longrightarrow NNH \longrightarrow N_2$	0.046
$NH_3 \longrightarrow NH_3(v_2) \longrightarrow NH_2 \longrightarrow H_2 NO \longrightarrow HNO \longrightarrow NO \longrightarrow NNH \longrightarrow N_2$	0.034
$NH_3 \longrightarrow NH_3(v_2) \longrightarrow NH_2 \longrightarrow H_2 NO \longrightarrow HNO \longrightarrow NO \longrightarrow N_2$	0.026
Cycles	Heating (W/cm ³)
$N_2 \longrightarrow N_2(v_2) \longrightarrow N_2$	239
$N_2 \longrightarrow N_2(v_6) \longrightarrow N_2$	195
$N_2 \longrightarrow N_2(B) \longrightarrow N_2$	172
$N_2 \longrightarrow N_2(v_3) \longrightarrow N_2$	169
$N_2 \longrightarrow N_2(v_4) \longrightarrow N_2$	155
$N_2 \longrightarrow N_2(v_5) \longrightarrow N_2$	139
$NH_3 \longrightarrow NH_3(v_2) \longrightarrow NH_3$	126
$N_2 \longrightarrow N_2(v_1) \longrightarrow N_2$	123
$N_2 \longrightarrow N_2(C) \longrightarrow N_2$	98
Total Heating	1416

Table 2Global pathways and cycles obtained using PGPA for the nanosecond discharge PAC of stoichiometric NH₃/air mixture at 550 Td. A positive value of heating denotes a net heat release through the pathway/cycle.

Global pathways/cycles	Parameter
Tracked by N atom	Dominance
$NH_3 \longrightarrow NH \longrightarrow N_2H_2 \longrightarrow NNH \longrightarrow N_2$	0.072
$NH_3 \longrightarrow NH_2 \longrightarrow H_2NO \longrightarrow HNO \longrightarrow NO \longrightarrow NNH \longrightarrow N_2$	0.068
$NH_3 \longrightarrow NH_3 + \longrightarrow NH_2 \longrightarrow H_2NO \longrightarrow HNO \longrightarrow NO \longrightarrow NNH \longrightarrow N_2$	0.057
$NH_3 \longrightarrow NH_3(v_2) \longrightarrow NH_2 \longrightarrow H_2NO \longrightarrow HNO \longrightarrow NO \longrightarrow NNH \longrightarrow N_2$	0.038
$NH_3 \longrightarrow NH_3(V_2) \longrightarrow NH_3 + \longrightarrow NH_2 \longrightarrow H_2 NO \longrightarrow HNO \longrightarrow NO \longrightarrow NNH \longrightarrow N_2$	0.036
$NH_3 \longrightarrow NH_3(v_2) \longrightarrow NH \longrightarrow N_2H_2 \longrightarrow NNH \longrightarrow N_2$	0.032
Cycles	Heating (W/cm ³)
$N_2 \longrightarrow N_2(C) \longrightarrow N_2$	697
$N_2 \longrightarrow N_2(B) \longrightarrow N_2$	355
$NH_3 \longrightarrow NH_3(v_2) \longrightarrow NH_3$	92
$N_2 \longrightarrow N_2(v_2) \longrightarrow N_2$	7.5
$N_2 \longrightarrow N_2(v_6) \longrightarrow N_2$	7.5
$N_2 \longrightarrow N_2(a') \longrightarrow N_2$	5.5
Total Heating	1164

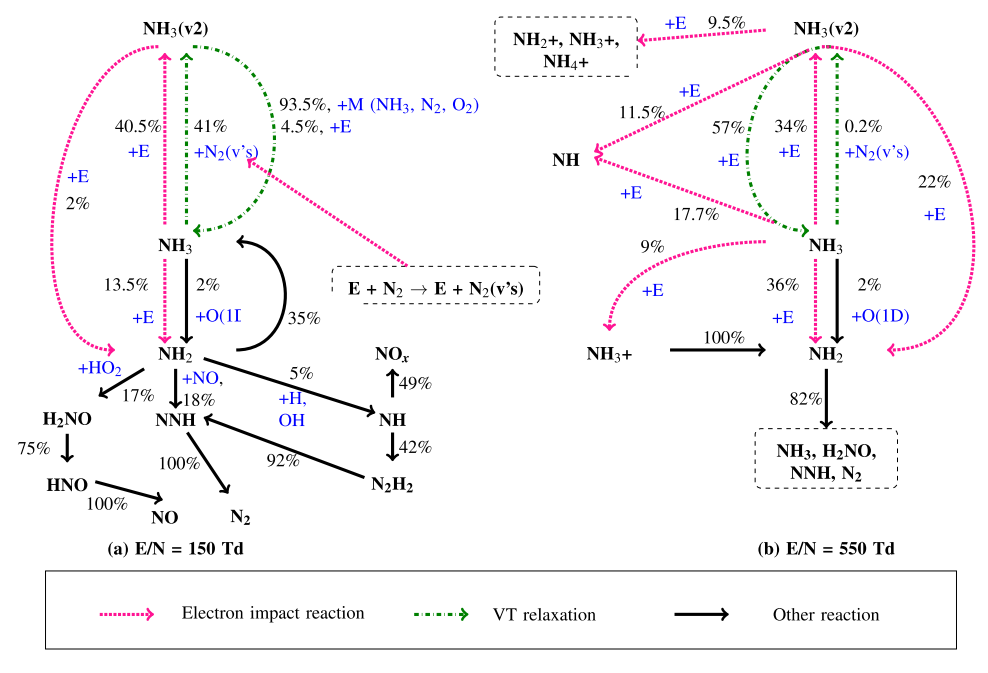


Fig. 5. Conventional path flux analysis for the consumption of NH_3 at E/N = (a) 150 Td and (b) 550 Td in a constant volume 0D batch reactor.

the ability of PGPA to accurately capture the global behavior of the PAC kinetics. A similar comparison between PGPA and PFA at 550 Td (see Fig. 5(b)) shows the ability of PGPA to identify the production of NH and NH_3^+ from NH_3 and the consumption of $NH_3(v_2)$ to produce other species (NH_3^+ , NH, etc.) in addition to NH_2 (compare Table 2 and Fig. 5(b)).

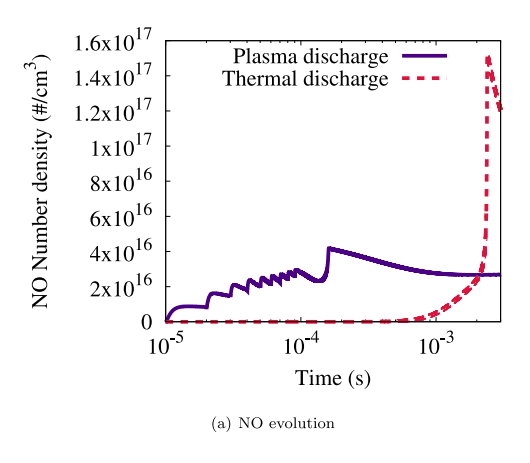
Similar to conventional PFA, PGPA is found to extract the global behavior in PAC kinetics. Nonetheless, PGPA offers a notable improvement in identifying specific reaction groups that are not part of any global pathways (V-T and electronic relaxations at 150 and 550 Td, respectively, See Tables 1 and 2), yet exhibiting an important role in reactivity. These reactions are not identified by conventional PFA, because these reactions can exist as isolated reactions (cyclic excitation and de-excitation reactions in PAC chemistry) that do not directly participate in the consumption of fuel. To sum up, PGPA can also extract information that PFA does not expose in a more precise and automatic manner. Additionally, unlike PFA, PGPA requires much less prior knowledge of chemical kinetics, making it a more accessible analysis tool.

4.2. NO_x production in plasma and thermal ignition

NH₃ combustion, when compared to conventional hydrocarbons, is carbon free and hence does not result in the production of CO₂. CO. and other unburnt hydrocarbons. The end products of a complete stoichiometric NH₃/air combustion is H₂O and N₂. Nevertheless, the fuel-bound nitrogen in NH3 can affect the production of NO_x, thereby resulting in significantly higher NO_x emissions compared to hydrocarbon combustion. Our recent study on the PAC of NH₃/air mixtures [29] observed the ability of plasmaassisted kinetics in reducing the fuel-bound NO_x emissions when compared to the NO_x production in conventional thermal energy deposition. The reduced production of NO_x in case of PAC was associated to the plasma-based reforming of NH₃ to N₂ and H₂ during the plasma discharges. This conclusion was arrived upon analyzing the system using multiple complicated path-flux analyses. One of the objectives of the current study is to analyze the production of NO_x using the PGPA, thereby circumventing the complexities of conventional path-flux analysis.

Figure 6 shows the evolution of NO and temperature in case of plasma discharge compared against thermal energy deposition for a stoichiometric NH3/air mixtures in a constant pressure 0D homogeneous batch reactor. The simulations are performed at 1 bar and an initial temperature of 800 K. A non-equilibrium plasma discharge at a frequency of 100 kHz, 10 pulses, with a pulse energy of 0.05 [/cm³ (0.5 [/cm³ in total) is used. On the other hand, a continuous deposition of 1.3 J/cm³ (a higher total energy) is used in case of thermal energy deposition in order to observe ignition. From Fig. 6, it can be observed that the plasma discharge case, regardless of being supplied with a lower total energy (0.5 J/cm³), exhibits an order of magnitude faster ignition compared to the thermal discharge case. In addition, a significant NO production is observed during plasma pulses ($< 9 \times 10^{-5}$) compared to almost zero NO production in case of thermal deposition. Despite higher reactivity and NO production during pulses, the plasma discharge case is found to produce a peak NO density of $\sim 4 \times 10^{16}$ (see Fig. 6(a)), which is about four times lower than that produced by the thermal discharge case ($\sim 1.5 \times 10^{17}$).

To understand the kinetics behind higher production of NO during pulses and lower production of peak NO at ignition in case of plasma discharges, PGPA is used to analyze the global pathways involving the production of NO during the early energy deposition phase (plasma/thermal energy deposition) and ignition. An element flux graph of N-atom is constructed for both plasma and thermal discharge case and global pathways are traced with NH₃ and NO as the source and sink species, respectively. Table 3



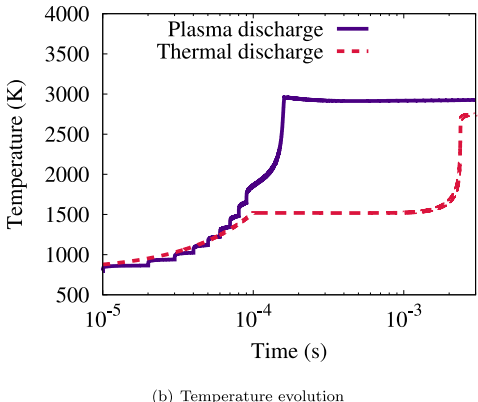


Fig. 6. Evolution of (a) number density of NO and (b) temperature for nanosecond plasma discharges (solid black line) and thermal energy deposition (dashed red line) in a constant pressure 0D batch reactor. (For interpretation of the references to color in this figure legend, the reader is referred to the web version of this article.)

shows the global pathways for the production of NO for plasma discharge case during both pulses ('Pulse' in Table 3) and ignition phase ('Ignition' in Table 3). Similarly, Table 4 depicts the NO production pathways for thermal discharge case during both thermal energy deposition phase ('TEDP' in Table 4, in which 'TEDP' stands for 'Thermal Energy Deposition Phase') and ignition ('Ignition' in Table 4). The identified global pathways are supplemented along with their NO production rates.

In case of plasma-assisted combustion, the NO production pathways during the pulses (see Table 3 - Pulse) are predominantly of the form $NH_3\longrightarrow NH_2\longrightarrow NH\longrightarrow N\longrightarrow N_2\longrightarrow N_2^*\longrightarrow NO$ where N_2^* represents the electronically excited states of N_2 ($N_2(A)$, $N_2(B)$, $N_2(a')$, and $N_2(C)$). However, in case of thermal energy-assisted combustion, the NO production pathways during the thermal energy deposition phase (see Table 4 - TEDP) are predominantly of the form $NH_3 \longrightarrow NH_2 \longrightarrow NH/HNO \longrightarrow NO$. Similar observations can be realized using conventional path-flux analysis as depicted in Fig. 7(a) and (b) for plasma and thermal energy deposition cases. These observation clearly indicate the early production of NO during plasma pulse to be N_2 -bound as, $N_2 \longrightarrow N_2^* \longrightarrow NO$ is observed to be the conversion step producing NO. Moreover, the rate of NO production during pulses is about 15 orders of magnitude higher compared to thermal energy deposition, owing to a faster NO formation channel through pathways involving N2 and its electronic states that are absent in thermal energy deposition, thereby explaining the larger production of NO during plasma pulses.

The NO production pathways at ignition for both plasma-assisted and thermal energy-assisted combustion are observed to be predominantly fuel-bound as NH_3 consumes to produce HNO followed by NO (see Tables 3 and 4 - Ignition). Similar observa-

Table 3Global reaction pathways for the production of NO in case of plasma-assisted ignition of a stoichiometric NH₃/air mixture at 1 bar and 800 K. The pathways are analyzed at the instances of plasma discharge and ignition.

Instance	Global NO production pathways	NO production (mol/cm ³ s)
Pulse	$NH_3 \longrightarrow NH_2 \longrightarrow NH \longrightarrow N \longrightarrow N_2 \longrightarrow N_2(a') \longrightarrow NO$	5.5×10^{-5}
	$NH_3 \longrightarrow NH_2 \longrightarrow NH \longrightarrow N \longrightarrow N_2 \longrightarrow N_2(B) \longrightarrow NO$	4.6×10^{-5}
	$NH_3 \longrightarrow NH_2 \longrightarrow NH \longrightarrow N \longrightarrow N_2 \longrightarrow N_2(C) \longrightarrow N_2(a') \longrightarrow NO$	4.5×10^{-5}
	$NH_3 \longrightarrow NH_2 \longrightarrow NH \longrightarrow N \longrightarrow N_2 \longrightarrow N_2(B) \longrightarrow N_2(A) \longrightarrow N_2(C) \longrightarrow N_2(a') \longrightarrow NO$	4.5×10^{-5}
	$NH_3 \longrightarrow NH_3(v_2) \longrightarrow NH_2 \longrightarrow NH \longrightarrow N \longrightarrow N_2 \longrightarrow N_2(a') \longrightarrow NO$	4.4×10^{-5}
	$NH_3 \longrightarrow NH_3(v_2) \longrightarrow NH_2 \longrightarrow NH \longrightarrow N \longrightarrow N_2 \longrightarrow N_2(B) \longrightarrow N_2(A) \longrightarrow N_2(C) \longrightarrow N_2(a') \longrightarrow NO$	3.9×10^{-5}
	Total production	$\sim 2.7 imes 10^{-4}$
Ignition	$NH_3 \xrightarrow{\sim} NH_2 \longrightarrow NH \longrightarrow HNO \longrightarrow NO$	1.3×10^{-4}
	$NH_3 \longrightarrow NH_2 \longrightarrow H_2NO \longrightarrow HNO \longrightarrow NO$	1.2×10^{-4}
	$NH_3 \longrightarrow NH_2 \longrightarrow NH \longrightarrow N \longrightarrow N_2 \longrightarrow NNH \longrightarrow HNO \longrightarrow NO$	9.3×10^{-5}
	$NH_3 \longrightarrow NH_2 \longrightarrow HNO \longrightarrow NO$	8.9×10^{-5}
	$NH_3^- \longrightarrow NH_2^- \longrightarrow NH \longrightarrow N_2O \longrightarrow N_2 \longrightarrow NNH \longrightarrow HNO \longrightarrow NO$	8.8×10^{-5}
	$NH_3 \longrightarrow NH_2 \longrightarrow H_2NO \longrightarrow HNOH \longrightarrow HNO \longrightarrow NO$	8.7×10^{-5}
	Total production	$\sim 7 imes 10^{-4}$

Table 4Global pathways for the production of NO in case of thermal energy-assisted ignition of a stoichiometric NH₃/air mixture at 1 bar and 800 K. The pathways are analyzed at the instances of thermal energy deposition and ignition. TEDP stands for 'Thermal Energy Deposition Phase'.

Instance	Global NO production pathways	NO production (mol/cm ³ s)
TEDP	$NH_3 \longrightarrow NH_2 \longrightarrow N_2H_3 \longrightarrow NH \longrightarrow NO$	1.2×10^{-19}
	$NH_3 \longrightarrow NH_2 \longrightarrow N_2H_4 \longrightarrow N_2H_3 \longrightarrow NH \longrightarrow NO$	1.3×10^{-20}
	$NH_3 \longrightarrow NH_2 \longrightarrow H_2NO \longrightarrow HNOH \longrightarrow HNO \longrightarrow NO$	1.2×10^{-20}
	$NH_3 \longrightarrow N_2H_3 \longrightarrow NH \longrightarrow NO$	6.1×10^{-21}
	$NH_3 \longrightarrow NH_2 \longrightarrow H_2NO \longrightarrow HNO \longrightarrow NO$	5.8×10^{-21}
	$NH_3 \longrightarrow NH_2 \longrightarrow N_2H_3 \longrightarrow NH \longrightarrow HNO \longrightarrow NO$	4.6×10^{-21}
	Total production	$\sim 1.6 imes 10^{-19}$
Ignition	$NH_3 \longrightarrow NH_2 \longrightarrow H_2NO \longrightarrow HNO \longrightarrow NO$	1.4×10^{-3}
	$NH_3 \longrightarrow NH_2 \longrightarrow NH \longrightarrow HNO \longrightarrow NO$	1.3×10^{-3}
	$NH_3 \longrightarrow NH_2 \longrightarrow HNO \longrightarrow NO$	1×10^{-3}
	$NH_3 \longrightarrow NH_2 \longrightarrow H_2NO \longrightarrow HNOH \longrightarrow HNO \longrightarrow NO$	9.3×10^{-4}
	$NH_3 \longrightarrow NH_2 \longrightarrow NH \longrightarrow N_2O \longrightarrow N_2 \longrightarrow NNH \longrightarrow HNO \longrightarrow NO$	9.1×10^{-4}
	$NH_3 \longrightarrow NH_2 \longrightarrow NH \longrightarrow N_2H_2 \longrightarrow NNH \longrightarrow HNO \longrightarrow NO$	8.6×10^{-4}
	Total production	$\sim 7 imes 10^{-3}$

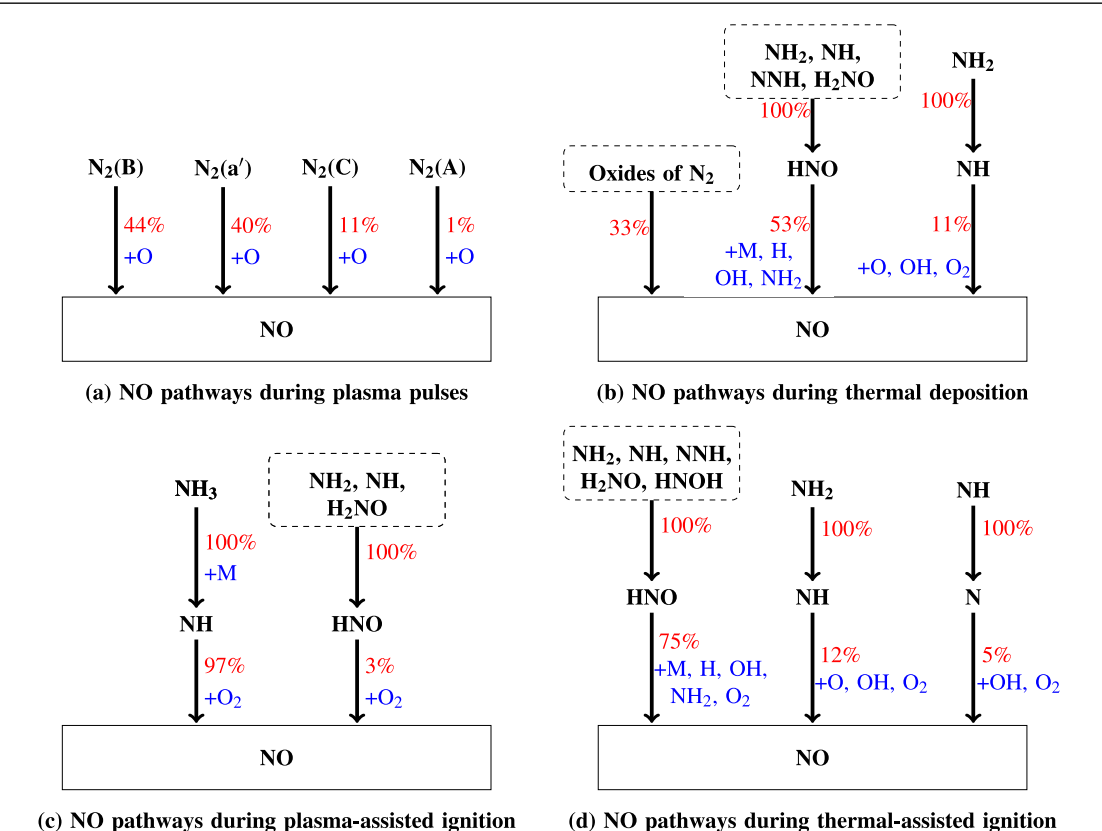


Fig. 7. Conventional path-flux analysis for the production of NO during (a) the plasma discharge pulses for plasma-assisted ignition, (b) the thermal energy deposition phase (TEDP) for thermal energy-assisted ignition, (c) the ignition phase of plasma-assisted ignition, and (d) the ignition phase of thermal energy-assisted ignition in a constant pressure 0D batch reactor. All percentages are relative to the produced species.

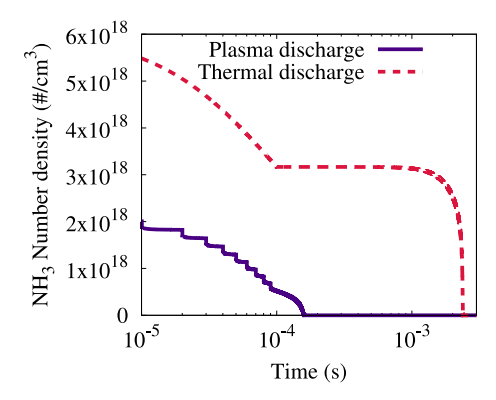


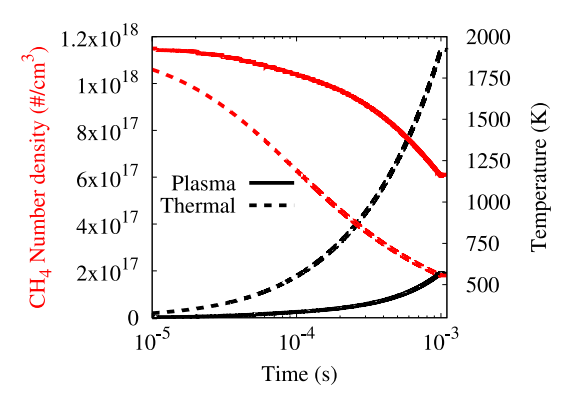
Fig. 8. Evolution of number density of NH₃ for nanosecond plasma discharges (solid black line) and thermal energy deposition (dashed red line) in a constant pressure 0D batch reactor. (For interpretation of the references to color in this figure legend, the reader is referred to the web version of this article.)

tions can be realized using conventional path-flux analysis as depicted in Fig. 7(c) and (d) for both plasma and thermal energyassisted ignition cases. Despite the similarity in pathways, the NO production rate for thermal energy-assisted case is an order of magnitude higher (7×10^{-3}) compared to plasma-assisted combustion (7 \times 10⁻⁴). This higher rate of NO production in the thermal energy-assisted case can be attributed to the higher levels of NH3 at ignition (see Fig. 8) thereby resulting in larger HNO and NO production compared to the plasma case. Specifically, the amount of NH3 at the instance of thermal energy-assisted ignition is about four times as that of plasma-assisted ignition, and is synonymous with the four times higher production of peak NO in thermal energy-assisted case compared to plasma-assisted case. The lower levels of NH₃ at the instance of ignition for plasmaassisted case can be ascribed to the early reforming of NH3 to N2 $(NH_3 \longrightarrow NH_2 \longrightarrow NH \longrightarrow N \longrightarrow N_2)$ during the plasma pulses (see Table 3 - Pulse), a phenomena which does not occur during the thermal energy deposition phase (TEDP).

Thus the PGPA analyses attributes the higher production of NO during plasma pulses to the plasma chemistry involving N_2 and its excited states and the lower production of peak NO for plasma-assisted combustion of NH_3 to the early reforming of NH_3 to N_2 and H_2 , resulting in a reduction of fuel-bound NO during ignition. The conventional path-flux analysis for NO production (as shown in Fig. 7) does not delineate the importance of early reforming of NH_3 in the reduction of peak NO, and therefore requires additional path-flux analysis for the consumption of NH_3 to uncover the effect of early reforming. Such analysis require certain pre-analysis intuitions, expert knowledge, and considerable human effort, making it laborious to obtain meaningful insights. Thus, the PGPA analyses are considerably automatic and requires lesser user-assistance when compared to path-flux analyses.

4.3. Plasma-assisted CH₄ reforming

To further validate the ability of PGPA in identifying the global pathways of plasma-assisted systems, the current study delves into the reforming of CH_4/N_2 mixtures using nanosecond plasma discharges and conventional thermal energy deposition. The pyrolysis mechanism by Mao et al. [44] $(CH_4/N_2/Ar/He$ pyrolysis chemistry) is used to simulate the reforming of CH_4 diluted by 40% N_2 at an initial temperature of 300 K and a pressure of 60 torr. The plasma-assisted reforming was performed at E/N of 100 Td, pulsing frequency of 100 kHz, and 100 pulses. While the plasma reforming was simulated using 0.3 mJ/cm³ per pulse (total energy = 30 mJ/cm³), a much higher total energy of 300 mJ/cm³ was used in thermal reforming so as to observe noticeable lev-



(a) CH₄ and Temperature

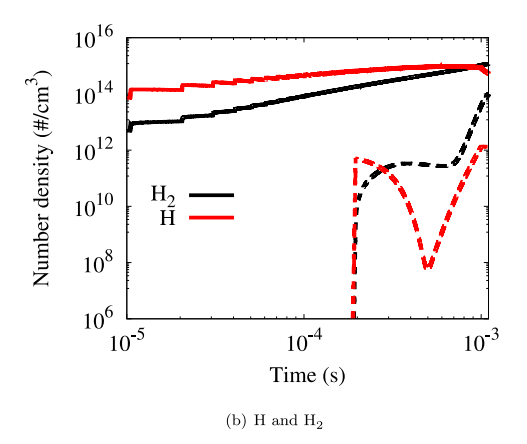


Fig. 9. Evolution of (a) CH_4 number density, temperature, and (b) number densities of H and H_2 for the pyrolysis of CH_4/N_2 mixture in a constant pressure 0D batch reactor at 60 torr and 300 K. The solid lines represent plasma-assisted reforming and the dashed lines depict thermal reforming.

els of hydrocarbon production. Figure 9 shows the evolution of temperature and number densities of CH₄, H₂, and H for both plasma (solid lines) and thermal reforming (dashed lines). At the end of energy deposition, the temperatures are found to be 570 K and 1920 K for plasma and thermal reforming, respectively. Despite the much lower final temperatures, plasma reforming exhibit an order of magnitude increased production of H₂ (\sim 1.1 \times 10¹⁵ molecules/cm³) as compared to thermal reforming (\sim 9 \times 10¹³ molecules/cm³) as observed in Fig. 9(b). In addition to the higher production of H₂, plasma reforming is also found to produce about two orders of magnitude higher levels of C₂ and C₃ species as shown in Fig. 10.

In order to understand the cause of increased CH₄ reforming during plasma discharges despite a much lower energy deposition, PGPA is used to analyze the production pathways of C₂H₆, C₂H₄, and C₂H₂. The reforming process involves the decomposition of parent species (CH₄) into smaller radicals (CH₃, CH₂, H, etc.) [45] and charged species with the latter in case of plasma reforming, and is followed by recombination and pyrolysis steps forming larger hydrocarbons and H2, respectively. Thus, it is essential to probe into the production rates of intermediate pyrolysis products to understand the dominance of one reforming technique over other. Table 5 shows the dominant global reaction pathways for the production of different C2 species along with the production rate of first intermediate species of the respective pathway for plasma and thermal reforming cases. The dominant production pathway for C_2H_6 is observed to be $CH_4 \rightarrow$ $\text{CH}_3 \longrightarrow \text{C}_2\text{H}_6$ for both plasma and thermal reforming. Regardless, the production rate of CH₃ (the first pyrolysis intermediate) is found to be about two orders of magnitude higher for plasma

Table 5

Dominant global reaction pathways for the production of different C_2 species along with the net production rate of first intermediate species in case of plasma- and thermal energy-assisted reforming of CH_4/N_2 mixture at 60 torr and 300 K. The pathways are analyzed at the instance of last plasma discharge pulse for both plasma and thermal reforming.

Assistance	Global C ₂ production pathways	Dominance	Species production (mol/cm³s)
Plasma	$CH_4 \longrightarrow CH_3 \longrightarrow C_2H_6$	0.46	4×10^{-4}
	$CH_4 \longrightarrow CH_2 \longrightarrow CH \longrightarrow C_2H_4 \longrightarrow C_2H_5 \longrightarrow CH_3 \longrightarrow C_2H_6$	0.42	1.4×10^{-5}
	$\operatorname{CH}_4 \longrightarrow \operatorname{CH}_4^+ \longrightarrow \operatorname{CH}_2 \longrightarrow \operatorname{CH} \longrightarrow \operatorname{C}_2\operatorname{H}_4$	0.38	1.4×10^{-5}
	$CH_4 \longrightarrow CH_3 \longrightarrow C_2H_6 \longrightarrow CH_2 \longrightarrow CH \longrightarrow C_2H_4$	0.33	2.8×10^{-4}
	$CH_4 \longrightarrow CH_4^+ \longrightarrow CH_2 \longrightarrow CH \longrightarrow C_2H_4 \longrightarrow aC_3H_4 \longrightarrow tC_3H_5 \longrightarrow C_2H_3 \longrightarrow H_2CC \longrightarrow C_2H_2$	0.22	8.2×10^{-6}
	$CH_4 \longrightarrow CH_4^+ \longrightarrow CH_2 \longrightarrow CH \longrightarrow C_2H_4 \longrightarrow aC_3H_4 \longrightarrow pC_3H_4 \longrightarrow tC_3H_5 \longrightarrow C_2H_3 \longrightarrow C_2H_2$	0.22	8.1×10^{-6}
Thermal	$CH_4 \longrightarrow CH_3 \longrightarrow C_2H_6$	0.4	2.2×10^{-6}
	$CH_4 \longrightarrow CH_3 \longrightarrow C_2H_5 \longrightarrow C_2H_6$	0.24	1.3×10^{-6}
	$CH_4 \longrightarrow CH_3 \longrightarrow C_2H_5 \longrightarrow C_2H_4$	0.9	4.9×10^{-6}
	$CH_4 \longrightarrow CH_3 \longrightarrow CH \longrightarrow C_2H_4$	0.2	1.1×10^{-6}
	$CH_4 \longrightarrow CH_3 \longrightarrow C_2H_5 \longrightarrow C_2H_4 \longrightarrow C_2H_2$	0.83	4.5×10^{-6}
	$CH_4 \longrightarrow CH_3 \longrightarrow CH \longrightarrow C_2H_4 \longrightarrow C_2H_2$	0.27	1.5×10^{-6}

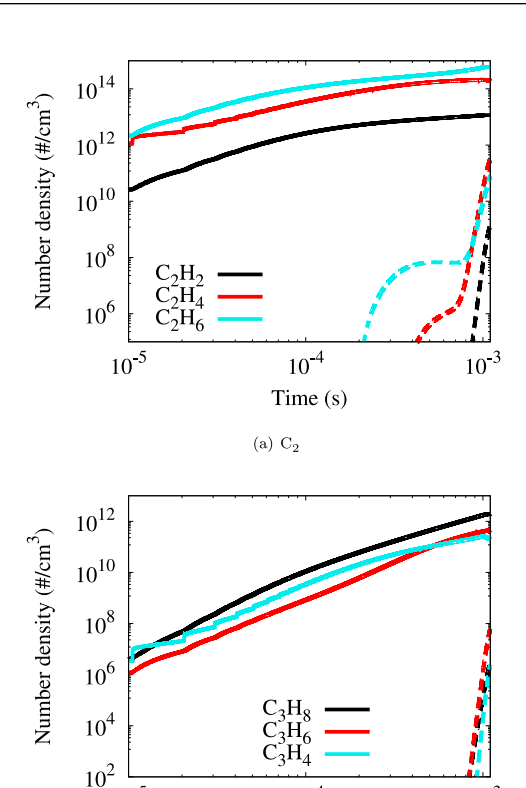


Fig. 10. Evolution of various (a) C_2 and (b) C_3 species for the pyrolysis of CH_4/N_2 mixture in a constant pressure 0D batch reactor at 60 Torr and 300 K. The solid lines represent plasma-assisted reforming, and the dashed lines depict thermal reforming.

(b) C₃

10-4

Time (s)

 10^{-3}

10⁻⁵

reforming $(4 \times 10^{-4} \text{ mol/cm}^3 \text{ s})$ compared to thermal reforming $(2.2 \times 10^{-6} \text{ mol/cm}^3 \text{ s})$. Thus, despite having same global pathways to produce C_2H_6 , the use of plasma clearly dominates over thermal reforming by producing larger quantities of CH_3 (see Fig. 11), followed by C_2H_6 . Further probing into details affecting the step $CH_4 \longrightarrow CH_3$ using PGPA, the major drivers of this step is found to be $CH_4 + N_2(e) \longrightarrow CH_3 + H + N_2(N_2(e) - \text{electronically excited states of } N_2)$ and $CH_4 + E \longrightarrow CH_3 + H + E$ for plasma reforming, whereas, $CH_4 + H \longrightarrow CH_3 + H_2$ for thermal reforming. This observation points to the dependence of thermal reforming on the H radical concentration, which itself is produced as part of CH_4 reforming. In presence of plasma discharges, the dependence of reforming on H radicals is eclipsed by more reactive plasma reac-

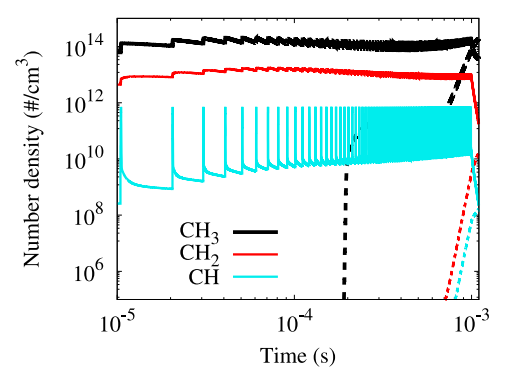
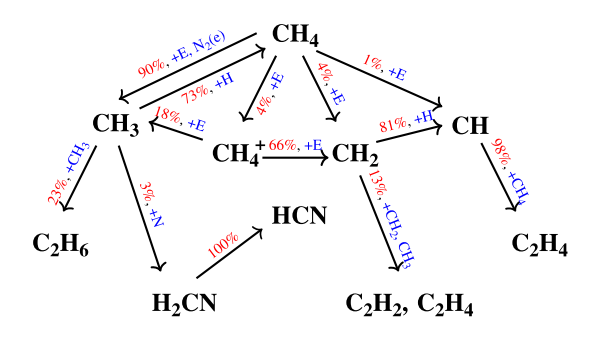


Fig. 11. Evolution of various radical species for the pyrolysis of CH_4/N_2 mixture in a constant pressure 0D batch reactor at 60 torr and 300 K. The solid lines represent plasma-assisted reforming and the dashed lines depict thermal reforming.

tions involving the electronically excited states of N_2 ($N_2(A)$, $N_2(B)$, etc.) and electron (E). The absence of these reactions in thermal case impedes the decomposition of CH_4 to CH_3 , thereby limiting the reforming of $CH_4 \longrightarrow C_2H_6$ as observed in Fig. 10(a).

Table 5 also lists the global reaction pathways producing C₂H₄ and C₂H₂, and exhibits higher production rates for intermediates (CH₃, CH₂, and CH₄⁺) for plasma case compared to thermal case (CH₃), thereby explaining the higher production of C₂H₄ and C₂H₂ in case of plasma discharges. To validate the aforementioned observations on the production of various C₂ species using PGPA, conventional path-flux analysis is performed for the consumption of CH₄ during plasma discharge and thermal energy deposition. Figure 12 portrays the path-flux analysis for the consumption of CH₄ during plasma and thermal energy deposition. For the plasma reforming (see Fig. 12(a)), it can be seen that the major first step in CH_4 reforming is $CH_4 \longrightarrow CH_3$ (~90%), of which ~73% goes back to CH₄ via H-addition. Majority of the remaining CH₃ (~23%) recombines to form C_2H_6 . This pathway $(CH_4 \longrightarrow CH_3 \longrightarrow C_2H_6)$ has been identified by PGPA as the major producer of C2H6 (see Table 5). Figure 12(a) also shows the importance of CH_4^+ , CH_2 , and CH in producing ethylene and acetylene, which are captured by global pathways in Table 5. In case of thermal reforming, majority of the CH₃ (~76%) proceeds to form C₂H₅, followed by C₂H₄ compared to CH_3 - CH_3 recombination (~16%). The global pathways identified by PGPA concurs with this observation, as the pathway $CH_4 \longrightarrow CH_3 \longrightarrow C_2H_5 \longrightarrow C_2H_4$ depicts a highest dominance of 0.9 and the largest production rate of CH₃ (4.9 \times 10⁻⁶ mol/cm³ s). Thus, the PGPA is able to identify the dominant pathways in producing various C2 species. Besides, PGPA is also able to identify additional pathways for the production of C2H2 from C2H4 for both plasma and thermal cases (see Table 5), which would require addi-



CH₄ Consumption during last pulse

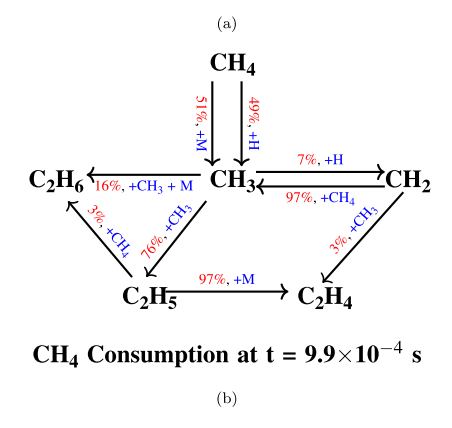


Fig. 12. Path-flux analyses for the consumption of CH_4 in (a) plasma and (b) thermal reforming of CH_4/N_2 mixture in a constant pressure 0D batch reactor at 60 torr and 300 K. All percentages are relative to the consumed parent species.

tional path-flux diagrams to be identified using conventional path-flux analysis. The global pathways for the production of different C_3 species are not included to account for the brevity of the present study.

In summary, PGPA is able to identify the global reaction pathways for the reforming of CH_4 to different species and has been validated using conventional path-flux analysis. These results for reforming, along with the PGPA and validations presented for NH_3 /air ignition (Section 4.1) and NO_x emissions (Section 4.2) buttress the ability of PGPA in identifying the global behavior of plasma-assisted systems and their analysis.

5. Conclusion

A Plasma-based Global Pathway Analysis (PGPA) has been developed based on existing Global Pathway Analysis (GPA) algorithm for conventional combustion systems (Gao et al. [21,25], Zhou and Yang [27]), extending the ability of existing algorithms to uncover various effects of plasma-based kinetics. Firstly, the GPA has been extended to identify the global reaction pathways based on element-flux graphs. Subsequently, a methodology based on depth first search (DFS) algorithm has been incorporated into PGPA, to identify cyclic channels involving the excitation and de-excitation of species critical to the reactivity. Quantifiable factors such as element flux dominance (based on elemental flux transfer), gas heating, and radical production have been integrated into PGPA to aid the analysis using global pathways and cycles by understanding their effects on reactivity.

The newly developed PGPA is then used to assess the global behavior of plasma-assisted systems and has been validated against the observations drawn using conventional path-flux analysis. In particular, three different problems have been analyzed:

- Firstly, the effect of gas heating due to vibrational-translational (V-T) relaxation on ignition of NH₃/air mixtures was analyzed at different reduced electric fields (E/N), with the V-T reactions found substantially boosting the reactivity at lower E/N. The prominence of specific reaction groups not part of any global pathways (V-T relaxation reactions) on the reactivity was made apparent using cyclic reactions identified by PGPA. The discovery of cyclic reactions is a notable improvement over traditional path-flux analysis (PFA), as, such reactions isolated from the main consumption channel of fuel are not identified by conventional path-flux analysis.
- The effect of plasma in reducing NO_x from NH₃/air mixtures has been discerned using PGPA by identifying the major NO production pathways. PGPA observed the early reforming of NH₃ to N₂ and H₂ to impede the production of NO during NH₃ ignition. On the contrary, PFA analysis requires considerable human effort, expert knowledge, and multiple path-flux analyses for the consumption of NH₃ to uncover the effect of early reforming. Thus, the ease of use and mostly automatic nature of PGPA analyses enable better insights into the intricacies of plasma chemistry.
- Finally, PGPA has been used to understand the role of electron impact dissociation of CH₄ in the improved reforming of CH₄/N₂ mixtures using plasma when compared to thermal reforming. Like the previous analyses, PGPA identified several new pathways for producing C₂H₂ from C₂H₄, requiring considerably less effort than PFA.

To sum up, the current study presents a better-automated analysis methodology to understand the intricacies involved in the reactivity of plasma-assisted kinetics with added insights compared to the traditional path-flux analysis. The newly developed methodology of PGPA and its insights can be utilized further to reduce the computational cost of plasma-assisted system simulation by formulating mechanism reduction strategies for plasma-based kinetic mechanisms.

Declaration of Competing Interest

The authors declare that they have no known competing financial interests or personal relationships that could have appeared to influence the work reported in this paper.

Acknowledgments

S. Yang acknowledges the grant support from NSF CBET 2002635. The information, data, or work presented herein was funded in part by the Advanced Research Projects Agency-Energy (ARPA-E), U.S. Department of Energy, under Award Number DE-AR0001529. The views and opinions of authors expressed herein do not necessarily state or reflect those of the United States Government or any agency thereof. P.N. Johnson acknowledges the graduate fellowship support from the Department of Mechanical Engineering at University of Minnesota. T.S. Taneja acknowledges the support from the UMII MnDrive Graduate Assistantship Award. The authors acknowledge Minnesota Supercomputing Institute (MSI) for the computational resources.

References

- A. Starikovskiy, N. Aleksandrov, Plasma-assisted ignition and combustion, Prog. Energy Combust. Sci. 39 (2013) 61–110.
- [2] S.M. Starikovskaia, Plasma assisted ignition and combustion, J. Phys. D 39 (2006) R265.
- [3] T. Ombrello, X. Qin, Y. Ju, A. Gutsol, A. Fridman, C. Carter, Combustion enhancement via stabilized piecewise nonequilibrium gliding arc plasma discharge, AIAA J. 44 (2006) 142–150.

- [4] G. Lou, A. Bao, M. Nishihara, S. Keshav, Y.G. Utkin, J.W. Rich, W.R. Lempert, I.V. Adamovich, Ignition of premixed hydrocarbon-air flows by repetitively pulsed, nanosecond pulse duration plasma, Proc. Combust. Inst. 31 (2007) 3327–3334.
- [5] W. Kim, M.G. Mungal, M.A. Cappelli, The role of in situ reforming in plasma enhanced ultra lean premixed methane/air flames, Combust. Flame 157 (2010) 374–383.
- [6] M. Scapinello, E. Delikonstantis, G.D. Stefanidis, The panorama of plasma-assisted non-oxidative methane reforming, Chem. Eng. Process. 117 (2017) 120–140.
- [7] Y. Ju, W. Sun, Plasma assisted combustion: dynamics and chemistry, Prog. Energy Combust. Sci. 48 (2015) 21–83.
- [8] T.Y. Chen, T.S. Taneja, A.C. Rousso, S. Yang, E. Kolemen, Y. Ju, Time-resolved in situ measurements and predictions of plasma-assisted methane reforming in a nanosecond-pulsed discharge, Proc. Combust. Inst. 38 (2021) 6533– 6540.
- [9] S.-H. Lam, D.A. Goussis, Understanding complex chemical kinetics with computational singular perturbation, Symp. (Int.) Combust. 22 (1989) 931–941. Elsevier
- [10] S.H. Lam, D.A. Goussis, The CSP method for simplifying kinetics, Int. J. Chem. Kinet. 26 (1994) 461–486.
- [11] T. Lu, Y. Ju, C.K. Law, Complex CSP for chemistry reduction and analysis, Combust. Flame 126 (2001) 1445–1455.
- [12] M. Valorani, H.N. Najm, D.A. Goussis, CSP analysis of a transient flame-vortex interaction: time scales and manifolds, Combust. Flame 134 (2003) 35–53.
- [13] U. Maas, S.B. Pope, Simplifying chemical kinetics: intrinsic low-dimensional manifolds in composition space, Combust. Flame 88 (1992) 239–264.
- [14] U. Maas, Efficient calculation of intrinsic low-dimensional manifolds for the simplification of chemical kinetics. Comput. Vis. Sci. 1 (1998) 69–81.
- [15] V. Bykov, U. Maas, Problem adapted reduced models based on reaction-diffusion manifolds (REDIMs), Proc. Combust. Inst. 32 (2009) 561–568.
- [16] T.F. Lu, C.S. Yoo, J.H. Chen, C.K. Law, Three-dimensional direct numerical simulation of a turbulent lifted hydrogen jet flame in heated coflow: a chemical explosive mode analysis, J. Fluid Mech. 652 (2010) 45–64.
- [17] S.H. Won, S. Dooley, F.L. Dryer, Y. Ju, A radical index for the determination of the chemical kinetic contribution to diffusion flame extinction of large hydrocarbon fuels, Combust. Flame 159 (2012) 541–551.
- [18] T. Turányi, Sensitivity analysis of complex kinetic systems. tools and applications, J. Math. Chem. 5 (1990) 203–248.
- [19] H. Zhong, M.N. Shneider, X. Mao, Y. Ju, Dynamics and chemical mode analysis of plasma thermal-chemical instability, Plasma Sources Sci. Technol. 30 (2021) 035002.
- [20] X. Gao, S. Yang, W. Sun, A global pathway selection algorithm for the reduction of detailed chemical kinetic mechanisms, Combust. Flame 167 (2016) 238–247.
- [21] X. Gao, S. Yang, W. Sun, Using global pathway to understand chemical kinetics, 6th International Workshop on Model Reduction in Reacting Flow, 2017.
- [22] W. Sun, Z. Chen, X. Gou, Y. Ju, A path flux analysis method for the reduction of detailed chemical kinetic mechanisms, Combust. Flame 157 (2010) 1298–1307.
- [23] X. Gao, W. Sun, Global pathway analysis of the autoignition and extinction of aromatic/alkane mixture, 53rd AIAA/SAE/ASEE Joint Propulsion Conference (2017), p. 4852.
- [24] S. Yang, X. Gao, W. Sun, Global pathway analysis of the extinction and re-ignition of a turbulent non-premixed flame, 53rd AIAA/SAE/ASEE Joint Propulsion Conference (2017), p. 4850.
- [25] X. Gao, X. Gou, W. Sun, Global pathway analysis: a hierarchical framework to understand complex chemical kinetics, Combust. Theor. Model. 23 (2019) 549–571

- [26] R. Mishra, A. Nelson, D. Jarrahbashi, Adaptive global pathway selection using artificial neural networks: a-priori study, Combust. Flame 244 (2022) 112279.
- [27] D. Zhou, S. Yang, Soot-based global pathway analysis: soot formation and evolution at elevated pressures in co-flow diffusion flames, Combust. Flame 227 (2021) 255–270.
- [28] P.N. Johnson, T.S. Taneja, S. Yang, Global pathway analysis of plasma assisted ammonia combustion, AIAA SCITECH 2022 Forum (2022), p. 0977.
- [29] T.S. Taneja, P.N. Johnson, S. Yang, Nanosecond pulsed plasma assisted combustion of ammonia-air mixtures: effects on ignition delays and NOx emission, Combust, Flame 245 (2022) 112327
- [30] A. Bellemans, N. Deak, F. Bisetti, Development of skeletal kinetics mechanisms for plasma-assisted combustion via principal component analysis, Plasma Sources Sci. Technol. 29 (2020) 025020.
- [31] A. Bellemans, N. Kincaid, N. Deak, P. Pepiot, F. Bisetti, P-DRGEP: a novel methodology for the reduction of kinetics mechanisms for plasma-assisted combustion applications, Proc. Combust. Inst. 38 (2021) 6631–6639.
- [32] G. Hagelaar, L.C. Pitchford, Solving the Boltzmann equation to obtain electron transport coefficients and rate coefficients for fluid models, Plasma Sources Sci. Technol. 14 (2005) 722.
- [33] I.V. Adamovich, W.R. Lempert, Challenges in understanding and predictive model development of plasma-assisted combustion, Plasma Phys. Control. Fusion 57 (2014) 014001.
- [34] M. Castela, B. Fiorina, A. Coussement, O. Gicquel, N. Darabiha, C.O. Laux, Modelling the impact of non-equilibrium discharges on reactive mixtures for simulations of plasma-assisted ignition in turbulent flows, Combust. Flame 166 (2016) 133–147.
- [35] L. Cheng, N. Barleon, B. Cuenot, O. Vermorel, A. Bourdon, Plasma assisted combustion of methane-air mixtures: validation and reduction, Combust. Flame 240 (2022) 111990.
- [36] C. Vázquez-Espí, A. Liñán, Fast, non-diffusive ignition of a gaseous reacting mixture subject to a point energy source, Combust. Theor. Model. 5 (2001) 485
- [37] D.L. Rusterholtz, D.A. Lacoste, G.D. Stancu, D.Z. Pai, C.O. Laux, Ultrafast heating and oxygen dissociation in atmospheric pressure air by nanosecond repetitively pulsed discharges, J. Phys. D 46 (2013) 464010.
- [38] S. Pancheshnyi, B. Eismann, G. Hagelaar, L.C. Pitchford, Computer Code ZD-PlasKin, University of Toulouse, Laplace, Technical Report, CNRS-UPS-INP, Toulouse, France, 2008. www.zdplaskin.laplace.univ-tlse.fr
- [39] R.J. Kee, F.M. Rupley, E. Meeks, J.A. Miller, CHEMKIN-III: A FORTRAN Chemical Kinetics Package for the Analysis of Gas-Phase Chemical and Plasma Kinetics, Technical Report, Sandia National Labs., Livermore, CA (United States), 1996.
- [40] X. Mao, Q. Chen, A.C. Rousso, T.Y. Chen, Y. Ju, Effects of controlled non-equilibrium excitation on H₂/O₂/He ignition using a hybrid repetitive nanosecond and DC discharge, Combust. Flame 206 (2019) 522–535.
- [41] J.K. Lefkowitz, P. Guo, A. Rousso, Y. Ju, Species and temperature measurements of methane oxidation in a nanosecond repetitively pulsed discharge, Philos. Trans. R. Soc. A 373 (2015) 20140333.
- [42] T.S. Taneja, S. Yang, Numerical modeling of plasma assisted pyrolysis and combustion of ammonia, AIAA Scitech 2021 Forum (2021), p. 1972.
- [43] G. Faingold, J.K. Lefkowitz, A numerical investigation of NH₃/O₂/He ignition limits in a non-thermal plasma, Proc. Combust. Inst. 38 (2021) 6661–6669.
- [44] X. Mao, Q. Chen, C. Guo, Methane pyrolysis with N₂/Ar/He diluents in a repetitively-pulsed nanosecond discharge: kinetics development for plasma assisted combustion and fuel reforming, Energy Convers. Manag. 200 (2019) 112018.
- [45] J.R. Fincke, R.P. Anderson, T. Hyde, B.A. Detering, R. Wright, R.L. Bewley, D.C. Haggard, W.D. Swank, Plasma thermal conversion of methane to acetylene, Plasma Chem. Plasma Process. 22 (2002) 105–136.